The EMBO Journal (2007), 1–11 | © 2007 European Molecular Biology Organization | All Rights Reserved 0261-4189/07
www.embojournal.org

THE EMBO JOURNAL

The structural basis of novel endosome anchoring activity of KIF16B kinesin

Nichole R Blatner[1], Michael I Wilson[2], Cai Lei[3], Wanjin Hong[3], Diana Murray[4], Roger L Williams[2] and Wonhwa Cho[1,*]

[1]Department of Chemistry, University of Illinois at Chicago, Chicago, IL, USA, [2]MRC Laboratory of Molecular Biology, Cambridge, UK, [3]Membrane Biology Laboratory, Institute of Molecular and Cell Biology, Singapore, Singapore and [4]Department of Microbiology and Immunology, Weill Medical College of Cornell University, New York, NY, USA

KIF16B is a newly identified kinesin that regulates the intracellular motility of early endosomes. KIF16B is unique among kinesins in that its cargo binding is mediated primarily by the strong interaction of its PX domain with endosomal lipids. To elucidate the structural basis of this unique endosomal anchoring activity of KIF16B-PX, we determined the crystal structure of the PX domain and performed *in vitro* and cellular membrane binding measurements for KIF16B-PX and mutants. The most salient structural feature of KIF16B-PX is that two neighboring residues, L1248 and F1249, on the membrane-binding surface form a protruding hydrophobic stalk with a large solvent-accessible surface area. This unique structure, arising from the complementary stacking of the two side chains and the local conformation, allows strong hydrophobic membrane interactions and endosome tethering. The presence of similar hydrophobic pairs in the amino-acid sequences of other membrane-binding domains and proteins suggests that the same structural motif may be shared by other membrane-binding proteins, whose physiological functions depend on strong hydrophobic membrane interactions.

The EMBO Journal advance online publication, 19 July 2007; doi:10.1038/sj.emboj.7601800
Subject Categories: membranes & transport; structural biology
Keywords: crystal structure; endosome anchoring; kinesin; PX domain

Introduction

Intracellular transport is essential for regulation of cellular morphology and function. Many of the steps in intracellular transport depend on active transport along the cytoskeleton, including actin filaments and microtubules. Microtubules form a dynamic and polarized cytoskeleton. In most cell types, microtubule plus ends grow dynamically toward the cell periphery from the microtubule-organizing centers near the nucleus that act as a cap of the minus ends. Transport of organelles and vesicles along the microtubule network is driven by two types of motor proteins; dyneins and kinesins (KIF) (Caviston and Holzbaur, 2006). While one major form of dynein is known to drive the minus end-directed transport of many different cargos, KIFs are an extended superfamily of microtubule motor proteins, many of which drive cargos toward the plus end (Miki *et al*, 2005; Caviston and Holzbaur, 2006).

The KIF superfamily is divided into 14 families, classified by both structure and function (Miki *et al*, 2005). All KIFs contain an approximately 360-residue catalytic core domain that is responsible for microtubule binding and ATP-dependant movement along the microtubules. For many KIFs, the conserved catalytic core is located at the N-terminal end, called the head region, which is followed by the neck region, the stalk region, and the tail region. The short neck region often contains family-specific features. Therefore, the catalytic core and the neck region, called the motor domain in combination, are well conserved in each family of KIFs, whereas the stalk/tail regions that are important for the interaction with other subunits of the holoprotein or with the cargo molecules such as proteins, lipids, and nucleic aids are highly divergent, even within the family. This structural diversity allows KIFs to be involved in a wide variety of cellular functions such as signal transduction, chromosome and organelle transport, microtubule depolymerization, and spindle formation. Kinesin-3 family members all have a characteristic β-sheet and α-helix in the neck region, followed by a fork-head-association domain (FHA) that has been implicated in intra- and intermolecular protein-protein interactions (see Figure 5A) (Westerholm-Parvinen *et al*, 2000; Lee *et al*, 2004). The kinesin-3 family comprises five major subfamilies (KIF1, KIF13, KIF14, KIF16, and KIF28), and an uncharacterized minor group, and most of them function in plus-end organelle transport (Miki *et al*, 2005).

The mechanisms by which KIFs interact with intracellular vesicles and organelles are still not fully understood. Although it was initially thought that KIFs directly interact with membrane-bound receptors on cargo, further studies have shown that many KIFs indirectly interact with cargo through one or more adaptor or scaffold proteins (Caviston and Holzbaur, 2006). Alternatively, KIFs can interact directly or indirectly with membrane lipids, phosphoinositides (PIs) in particular, on vesicles or organelles. Three members of kinesin-3 family have been reported to follow this mechanism. GAKIN/KIF13B indirectly interacts with phosphatidylinositol-3,4-5-trisphosphate (PtdIns(3,4,5)P_3)-containing vesicles by interacting with PIP_3BP/centaurin-α that binds PtdIns(3,4,5)P_3 through one of its PH domains (Horiguchi *et al*, 2006). KIF1A/UNC-104 contains a PH domain in its tail region that specifically interacts with phosphatidylinositol-4,5-bisphosphate (PtdIns(4,5)P_2)-enriched rafts in synaptic vesicles (Klopfenstein *et al*, 2002). Most recently, KIF16B was found to harbor a C-terminal PX domain that can bind to

*Corresponding author. Department of Chemistry (M/C 111), University of Illinois at Chicago, 845 West Taylor Street, Chicago, IL 60607, USA. Tel.: +1 312 996 4883; Fax: +1 312 996 0431; E-mail: wcho@uic.edu

Received: 22 March 2007; accepted: 26 June 2007

phosphatidylinositol-3-phosphate (PtdIns(3)P)-containing early endosomes, and thereby regulate the plus-end motility of early endosomes (Hoepfner *et al*, 2005). This endosomal transport process, which is regulated by the small GTPase Rab5 and PI 3-kinase hVPS34, is important for modulating the intracellular localization of early endosomes and balancing between receptor recycling and degradation. Since the depletion of cellular PtdIns(3)P abrogates the KIF16B-mediated endosomal transport (Hoepfner *et al*, 2005), the PtdIns(3)P-PX interaction seems to be the primary KIF–cargo interaction for this process. This raises a question as to how PtdIns(3)P-mediated membrane interactions of KIF16B-PX ensure tight binding between a KIF16B molecule and a bulky early endosome throughout the transport along microtubules.

PX domains are structural modules of 100–120 amino acids that have been shown to bind a variety of PIs and/or proteins and regulate the subcellular localization and function of proteins in which they reside (Wishart *et al*, 2001; Birkeland and Stenmark, 2004; Cho and Stahelin, 2005; Seet and Hong, 2006). Crystal and solution structures of multiple PX domains have shown that these domains have a common structural fold consisting of a twisted three-stranded β-sheet on one side of the module, with a minimum of three α-helices clustered together on the other side, forming a basic PI-binding pocket (Bravo *et al*, 2001; Karathanassis *et al*, 2002; Lu *et al*, 2002; Zhou *et al*, 2003; Xing *et al*, 2004; Stahelin *et al*, 2006). As is the case with other lipid-binding domains, membrane-binding surfaces of PX domains surrounding the PI-binding pocket contain cationic and hydrophobic residues. It has been reported that binding of a specific PI to the pocket induces the membrane penetration of the hydrophobic residues, which results in increased membrane affinity and sustained membrane residence (Stahelin *et al*, 2002, 2003a; Cho and Stahelin, 2005).

To understand the mechanism by which KIF16B tightly binds early endosomes via its PX domain, thereby regulating the motility of early endosomes, we determined the crystal structure of the KIF16B-PX domain and investigated the interactions of the full-length KIF16B, the PX domain, and their respective mutants with PtdIns(3)P-containing vesicles and cellular early endosomes. Results show that the PX domain contains two neighboring hydrophobic residues, L1248 and F1249, on the membrane-binding surface, which have a unique orientation and a large solvent-accessible surface area that allows these residues to penetrate into the hydrocarbon region of PtdIns(3)P-containing membranes and tether the PX domain to early endosomes.

Results

Membrane binding properties of the KIF16B-PX domain

Early endosomes are known to be enriched in PtdIns(3)P (Gillooly *et al*, 2000). Thus, for the PX domain (residues 1179–1317) of KIF16B to serve as anchor during the transport of early endosomes along microtubules, it should have high affinity for PtdIns(3)P-containing vesicles. Although it was previously reported that KIF16B-PX binds vesicles containing some 3-PIs (Hoepfner *et al*, 2005), the PI specificity and membrane affinity of KIF16B-PX have not been rigorously determined. We therefore measured by the SPR analysis, the affinity of KIF16B-PX for POPC/POPE/PI (77:20:3) vesicles, containing each of seven PIs, coated on the sensor chip. As shown in Figure 1A, KIF16B-PX is selective for PtdIns(3)P, although it can also bind other 3-PIs, including PtdIns(3,4)P_2, PtdIns(3,5)P_2, and PtdIns(3,4,5)P_3. It showed no detectable affinity for other PIs. The equilibrium SPR analysis (Figure 1B) yielded the K_d values for vesicles containing 3 mol% PtdIns(3)P, PtdIns(3,4)P_2, PtdIns(3,5)P_2, and PtdIns(3,4,5)P_3 as 2.7, 28, 310, and 100 nM, respectively (Table I). The K_d of KIF16B-PX for POPC/POPE/PtdIns(3)P (77:20:3) vesicles is comparable to those of the highest-affinity PtdIns(3)P-binding domains characterized so far, including $p40^{phox}$ PX domain (Stahelin *et al*, 2003a) and endofin FYVE domain (Blatner *et al*, 2004), both of which were shown to autonomously target early endosomes when expressed in mammalian cells. These results thus show that

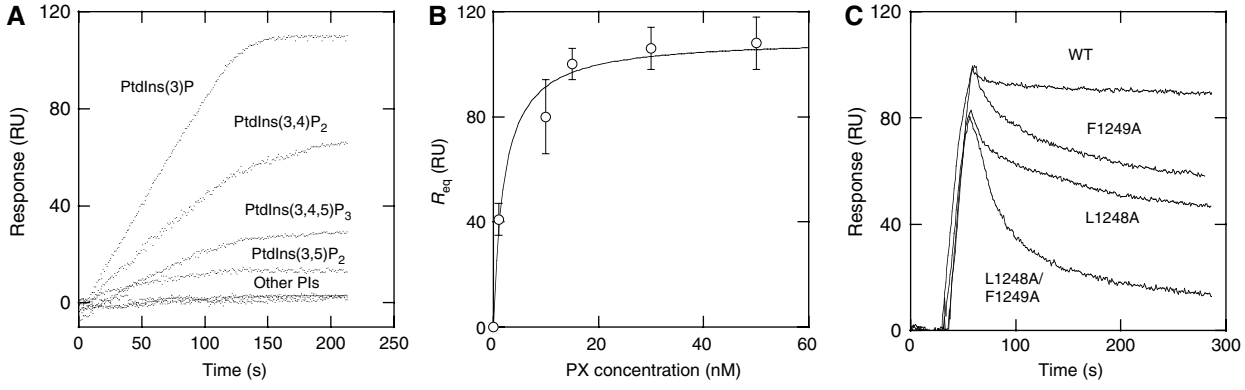

Figure 1 SPR sensorgrams for KIF16B-PX membrane binding. (**A**) PI specificity of the KIF16B-PX domain. The PX domain (100 nM) was injected over the sensor chip coated with various POPC/POPE/PI (77:20:3) vesicles. PIs include PtdIns(3)P, PtdIns(4)P, PtdIns(5)P, PtdIns(3,4)P_2, PtdIns(3,5)P_2, PtdIns(4,5)P_2, and PtdIns(3,4,5)P_3. The SPR response curves for respective PI are shown after background correction for binding to the control surface coated with POPC/POPE (80:20), which was minimal. (**B**) A binding isotherm generated from the R_{eq} (average of triplicate measurements) versus the concentration of the KIF16B-PX domain plot. A solid line represents a theoretical curve constructed from R_{max} ($=110\pm5$) and K_d ($=2.7\pm0.6$ nM) values determined by non-linear least-squares analysis of the isotherm, using the equation: $R_{eq}=R_{max}/(1+K_d/C)$. R_{eq} values were obtained from the equilibrium SPR measurements using 1–50 nM of the KIF16B-PX domain and the surface coated with POPC/POPE/PtdIns(3)P (77:20:3) vesicles. (**C**) Kinetic SPR sensorgrams for the KIF16B-PX domain and three mutants, F1249A, L1248A, and L1248A/F1249A interacting with the surface coated with POPC/POPE/PtdIns(3)P (77:20:3) vesicles. A 20 mM Tris buffer solution, pH 7.4, with 0.16 M KCl, was used for all measurements.

Table I Membrane binding of KIF16B PX domain and mutations to POPC/POPE/PI (77:20:3) vesicles determined by SPR analysis[a]

Proteins	PI used	K_d (M)	Fold increase in K_d[b]
KIF16B-PX	PtdIns(3)P	$(2.7 \pm 0.6) \times 10^{-9}$	1
KIF16B-PX	PtdIns(3,4)P_2	$(2.8 \pm 1.0) \times 10^{-8}$	10
KIF16B-PX	PtdIns(3,4,5)P_3	$(1.0 \pm 0.4) \times 10^{-7}$	37
KIF16B-PX	PtdIns(3,5)P_2	$(3.1 \pm 0.2) \times 10^{-7}$	115
R1220A	PtdIns(3)P	NM[c]	>1000
R1225A/K1229A/K1232A	PtdIns(3)P	$(8.5 \pm 1.4) \times 10^{-9}$	3
L1248A	PtdIns(3)P	$(1.8 \pm 0.3) \times 10^{-8}$	7
L1248V	PtdIns(3)P	$(1.6 \pm 0.1) \times 10^{-8}$	6
F1249A	PtdIns(3)P	$(1.3 \pm 0.3) \times 10^{-8}$	5
L1248A/F1249A	PtdIns(3)P	$(6.8 \pm 1.0) \times 10^{-8}$	25
L1248F/F1249L	PtdIns(3)P	$(3.3 \pm 1.2) \times 10^{-9}$	1.2
R1260A	PtdIns(3)P	$(8.0 \pm 5.0) \times 10^{-8}$	30

[a]All measurements were performed in 20 mM Tris, pH 7.4, containing 0.16 M KCl.
[b]Fold increase in K_d with respect to the wild-type PX domain with POPC/POPE/PtdIns(3)P (77:20:3) vesicles.
[c]Not measurable.

KIF16B-PX can bind PtdIns(3)P-containing vesicles with high affinity and significant specificity, which should help KIF16B translocate and tightly bind to early endosomes.

Structure of the KIF16B-PX domain

To understand the structural basis for the PI selectivity and high membrane affinity of KIF16B-PX, we used X-ray diffraction to determine its crystal structure (PDB ID: 2v14). The structure of KIF16B-PX was solved using MAD for phasing the diffraction data (Table II). The resulting electron density map was easily interpretable (Supplementary Figure 1). The structure, refined to 2.2 Å, has all the hallmarks of a canonical PX domain (Bravo *et al*, 2001), consisting of a twisted three-stranded β-sheet flanked along its length by an α-helix and a polyproline (PP_{II}) helix (residues 1243–1245) containing loop, with a second helix filling the hollow of the concave structure (Figure 2A). The bulge of β1 (residues 1189–1190) that displaces the β1–β2 loop from the PP_{II}–α2 loop, forming the PI-binding site, is conserved as in other PX domains. The α1–PP_{II} loop is shorter than in other PX domains, and this tighter turn toward the head of α2 results in a flatter membrane-binding surface. Although the arrangement of C-terminal loops and short helices following α2, including a 3_{10} helix α4, differs markedly from that seen in other PX domains, it succeeds in filling what remains of the hydrophobic concavity formed by the β-sheet, α2 and α3, as in other PX domains. In addition, two smaller hydrophobic pockets are formed by this arrangement, one between the N-terminus of β1 and C-terminus of α2, and another consisting of a cluster of six leucines from the α2–α3 and β2–β3 loops. In the crystals of KIF16B-PX, a pair of hydrophobic residues, L1248–F1249, sits in one of these pockets on an adjacent molecule. This crystal contact partially occludes the lipid-binding site, making it unlikely that lipid tails could be accommodated in this crystal form. Indeed 500 μM di-C_4 PtdIns(3,4,5)P_3, which was present in the crystallization condition, was not seen in the structure. Also, crystals soaked in solutions containing diC_4-PtdIns(3)P, inositol-1,3,4,5-tetrakisphosphate, or inositol-1,3,4-trisphosphate did not yield PX–lipid or inositol complexes.

Although positions of R1220 and Y1221 are almost identical to the key 3-phosphate-binding residues R58 and Y59 of p40^{phox}-PX (Figure 2B), as are three water molecules in the lipid-binding pocket, with a fourth water molecule occupying the position of the 3-phosphate of PtdIns(3)P in the p40^{phox}-PX structure, the PI-binding pocket of KIF16B-PX is more open than that of p40^{phox}-PX. The presence of a serine residue, S1222, in KIF16B-PX at the position equivalent to the 1-phosphate ligand of PtdIns(3)P in p40^{phox}-PX (R60) removes part of the lateral wall of the binding pocket and may allow for repositioning of the PtdIns(3)P 1-phosphate to interact with R1225 one turn further down α1 in KIF16B-PX. The other side of the pocket is opened up by the repositioning of the R1260 side chain, equivalent to R105 in p40^{phox}-PX that interacts with the 4- and 5-OH of PtdIns(3)P, as a result of the H-bond it makes with N1251. This pocket widening may explain the capacity of KIF16B-PX to bind PtdIns(3,4)P_2, PtdIns(3,5)P_2, and PtdIns(3,4,5)P_3 headgroups in addition to PtdIns(3)P. It was reported that the PP_{II}–α2 loop of Grd19p PX domain is flexible and does move laterally in the presence of PtdIns(3)P when compared to the unliganded

Table II Data collection, phasing, and refinement statistics for MAD (SeMet)

	SeMet KIF16B	
Data collection		
Space group	I23	
Cell dimensions	$a = b = c = 100.9$ Å	
	Peak	Remote
Wavelength	0.979	0.9393
Resolution (Å)	2.2	2.8
R_{sym} or R_{merge}	0.095 (0.46)[a]	0.095 (0.48)
$I/\sigma I$	29.8 (2.2)	35.7 (6.4)
Completeness (%)	100 (100)	100 (100)
Multiplicity	27.5 (5.2)	20.5 (21.5)
Refinement		
Resolution (Å)	71.4–2.2	
Number of reflections	8819	
R_{work}/R_{free}	0.21/0.29	
Number of atoms	1180	
Protein	1118	
Water	62	
B-factors		
Protein	39.2	
Water	41.2	
R.m.s.ds		
Bond lengths (Å)	0.012	
Bond angles (deg)	1.38	

[a]The highest-resolution shell is shown in parenthesis.

state (Zhou *et al*, 2003). Similar movement of the loop in KIF16B-PX might also help binding of larger PI headgroups to the pocket.

The most novel feature of KIF16B-PX is a pair of hydrophobic residues, L1248 and F1249, on the PP_{II}–α2 loop. Although such hydrophobic pairs on the PP_{II}–α2 loop are also found in other PX domain structures, such as $p40^{phox}$ and PI3K-C2α, it is the local conformation of KIF16B-PX that makes it unique among PX domains. That is, the PP_{II}–α2 loop of KIF16B-PX adopts a tight turn with L1248/F1249 at its apex facing into the solvent (Figure 2B). This tight turn arises from a glycine residue, G1250, in a left-handed helical conformation, that follows the L1248/F1249 pair, and the hydrogen bonds between the side chains of R1260, T1251 and the K1247 main chain that constrain the loop. As a result, two side chains stack onto each other and form a hydrophobic stalk (Figure 2C), with a total solvent-accessible surface area of 272 $Å^2$. This large surface is completely apolar and the maximal binding energy upon burial of this hydrophobic surface in a lipid bilayer may reach 3.5 kcal/mol according to the hydrophobicity index of amino acids by Wimley and White (1996). The orientation of these two neighboring hydrophobic residues, which maximizes membrane penetration, is unique among PX domain structures and other lipid-binding domains characterized so far.

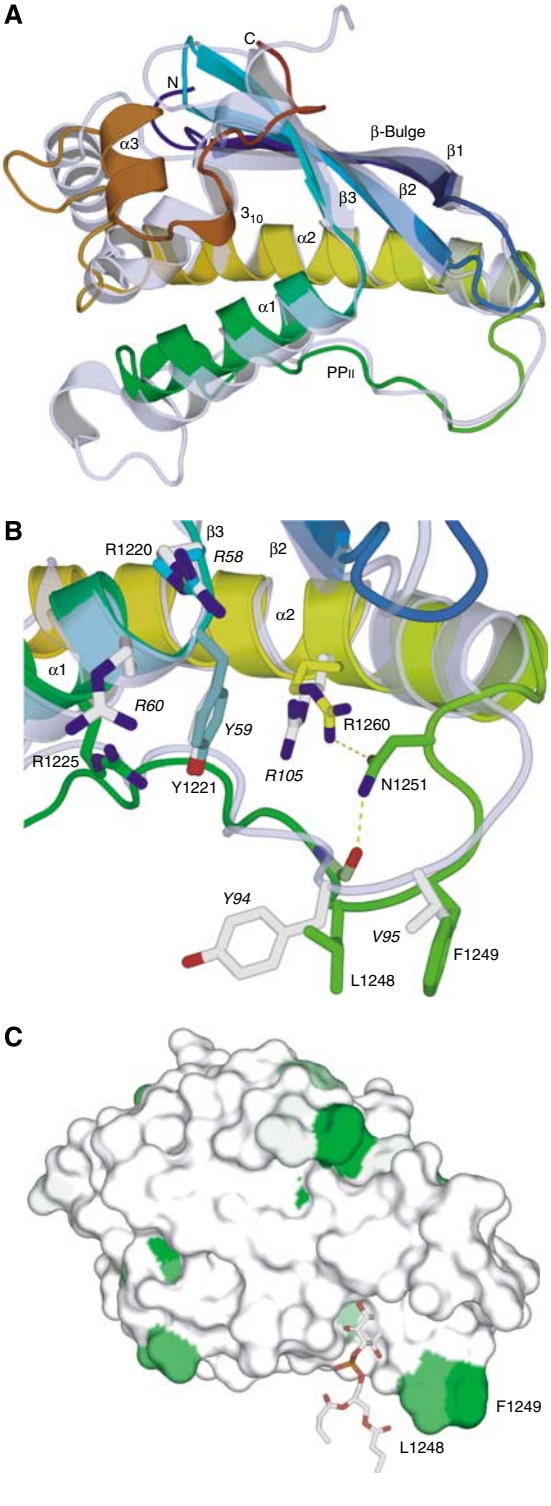

Figure 2 The overall structure of KIF16B-PX (PDB ID: 2v14). (**A**) A ribbon representation of the secondary structure of KIF16B-PX (rainbow colors) superimposed on $p40^{phox}$-PX shown in semi-transparent blue ribbons (r.m.s.d. = 1.0 Å for 52 Cα atoms). (**B**) PtdIns(3)P-binding residues of $p40^{phox}$-PX, shown as CPK-colored sticks with italicized labels, superimposed as in panel A with equivalent residues in KIF16B-PX shown as rainbow-colored sticks. The hydrogen bonds to N1251 side chain in the KIF16B-PX PP_{II}–α2 loop are shown as dotted lines. (**C**) Surface representation of KIF16B-PX with hydrophobic side chains colored from least to greatest side chain solvation free energy (Wimley and White, 1996) by increasing shades of green. The position of PtdIns(3)P is shown from structural alignment with $p40^{phox}$-PX as in panel A. Main chain atoms are colored white. Illustrations were created with PyMOL.

Roles of exposed hydrophobic residues in membrane binding of KIF16B-PX

To determine the roles of these unique hydrophobic residues in the membrane binding of KIF16B-PX, we measured the membrane binding properties of the KIF16B-PX domain and mutants (L1248A, L1248V, F1249A, and L1248A/F1249A) by SPR and monolayer penetration analyses. First, we determined the affinities of these proteins for POPC/POPE/PtdIns(3)P (77:20:3) vesicles immobilized onto the sensor surface by SPR analysis (Table I). L1248A, L1248V, and F1249A have 7-, 6-, and 5-fold lower affinity than the wild type, respectively, whereas a double mutant L1248A/F1249A shows 25-fold lower affinity than the wild type. It is interesting to find that the L1248V mutation, which is expected to reduce the solvent-accessible surface area of the side chain only by 4% (Chothia, 1974), reduces the membrane affinity of KIF16B-PX as much as the L1248A mutation. This implies that the complementarity between L1248 and F1249 side chains is important for maintaining the unique local conformation of KIF16B-PX that is optimized for membrane penetration (see below). The loss of binding energy due to the L1248A/F1249A mutation, estimated using an equation; $\Delta\Delta G^0 = -RT\ ln\ (K_d$ for WT/K_d for mutant), is 1.9 kcal/mol at 23°C. Taking into account that the L1248A/F1249A mutation would reduce the total surface area of the two side chains by about 54% (Chothia, 1974), this binding energy value suggests that the protruding hydrophobic residues are fully inserted into the membrane, thereby anchoring the PX domain to the membrane. Thus, the unique orientation of the L1248/F1249 side chains apparently optimizes the membrane penetration of these hydrophobic side chains.

To further test this notion, we performed two independent measurements. First, we monitored by SPR analysis the kinetics of membrane association and dissociation of KIB16B-PX, and mutants using POPC/POPE/PtdIns(3)P vesicles coated onto the sensor chip. As shown in Figure 1C, the wild-type KIF16B-PX displayed rapid membrane association followed by extremely slow dissociation. Even after exhaustive elution (i.e., >20 min), $>80\%$ of the protein remained on the surface (data not shown), which made it impractical to accurately determine the dissociation rate constant (k_{off}). Mutations of L1248 and F1249 greatly influenced the membrane dissociation of KIF16B-PX, while having a much lesser effect on membrane association. As a result, all mutants dissociated from the surface much more rapidly than the wild type. Graphical estimation of k_{off} values indicates that the L1248A/F1248A mutant has >50-fold higher k_{off} than KIF16B-PX.

We then measured the interactions of KIF16B-PX and mutants with phospholipid monolayers at the air–water interface. A monolayer composed of either POPC/POPE (80/20) or POPC/POPE/PtdIns(3)P (77:20:3) at a given π_0 was spread at a constant area, and the change in surface pressure ($\Delta\pi$) was monitored after the protein was injected into the subphase. As seen in Figure 3A, KIF16B-PX has significant penetration activity toward the neutral POPC/POPE (80/20) monolayer, with $\pi_c \approx 30$ dyne/cm. This activity is clearly higher than other PX domains, including p40^{phox}-PX, indicating high intrinsic membrane-penetrating activity of KIF16B-PX. Intriguingly, incorporation of 3 mol % PtdIns(3)P into the monolayer (i.e., POPC/POPE/PtdIns(3)P (77:20:3)) allowed KIF16B-PX to penetrate the monolayer with $\pi_c \approx 35$ dyne/cm. Since the surface pressure of cell membranes has been estimated to be between 31–35 dyne/cm (Demel *et al*, 1975; Marsh, 1996), this implies that KIF16B-PX has an ability to effectively penetrate PtdIns(3)P-containing endosomes. Mutation of L1248 and/or F1248 significantly reduced the penetration of KIF16B-PX into the POPC/POPE/PtdIns(3)P (77:20:3) monolayer with $\pi_c \leqslant 30$ dyne/cm (Figure 3C), corroborating the notion that these hydrophobic residues are directly involved in membrane penetration. Even with the POPC/POPE (80/20) monolayer, L1248A and F1248A mutations considerably weakened the penetration activity of KIF16B-PX (Figure 3D). Collectively, these SPR and monolayer penetration results show that two neighboring hydrophobic residues, L1248 and F1249, effectively penetrate the membrane, thereby providing extra membrane binding

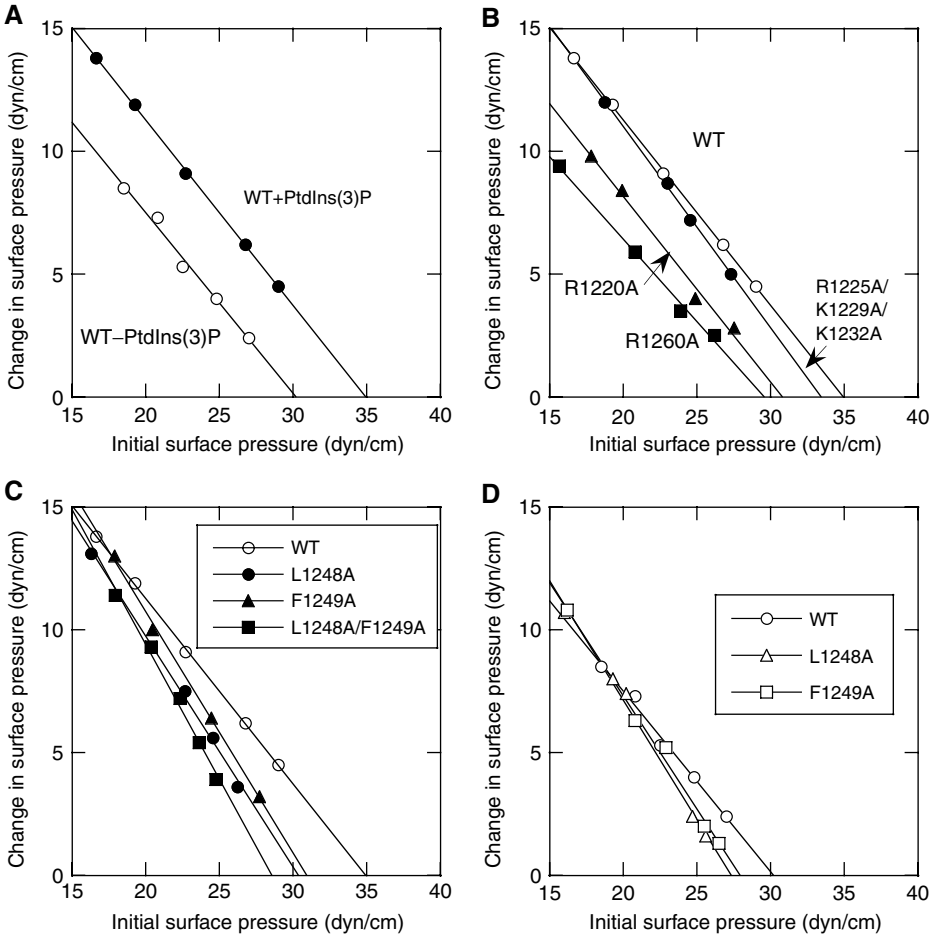

Figure 3 Monolayer penetration of KIF16B-PX wild type and mutations. (**A**) Interaction of KIF16B-PX with POPC/POPE (80:20) (○) and POPC/POPE/PtdIns(3)P (77:20:3) (●) monolayers as a function of π_0. (**B**) Interaction of KIF16B-PX (○), R1220A (▲), R1260A (■), and R1225A/K1229A/K1232A (●) mutants with the POPC/POPE/PtdIns(3)P (77:20:3) monolayer. (**C**) Interaction of KIF16B-PX (○), L1248A (●), F1249A (▲), and L1248A/F1249A (■) with POPC/POPE/PtdIns(3)P (77:20:3) monolayers. L1248V behaved essentially the same as L1248A. (**D**) Interaction of KIF16B-PX (○), L1248A (△), and F1249A (□) with the POPC/POPE (77:20:3) monolayer. The protein concentration in the subphase that yielded the saturating $\Delta\pi$ varied between 0.5 and 1 μg/ml depending on the π_0 of the lipid monolayer.

energy necessary for KIF16B-PX to stay on the membrane for an elongated period.

Roles of cationic residues in membrane binding of KIF16B-PX

As described above, our crystal structure suggests that a few cationic residues (i.e., R1220, R1260, and possibly R1225) of KIF16B may be involved in PI headgroup recognition. KIF16B-PX also contains a cluster of basic residues (K1229 and K1232 that are adjacent to R1225) on the membrane-binding side of helix α1, that could aid to enhance the membrane association of KIF16B-PX domain through non-specific electrostatic interactions. We determined the roles of these cationic residues by measuring the effects of their mutations on membrane binding. First, the affinities of the wild type and mutants for POPC/POPE/PtdIns(3)P (77:20:3) vesicles coated on to the sensor chip were measured by SPR analysis. As summarized in Table I, R1220A showed no detectable affinity, supporting the notion that this is a critical residue for PtdIns(3)P binding. R1260A also had greatly reduced (i.e., 30-fold) affinity for PtdIns(3)P-containing vesicles, suggesting that R1260 be directly involved in PI recognition, probably interacting with 4- and 5-OH in case of PtdIns(3)P or 4- and 5-phosphate in case of PtdIns(3,4)P_2, PtdIns(3,5)P_2, and PtdIns(3,4,5)P_3. This notion was supported by the finding that R1260A showed undetectable affinity for both PtdIns(3,4)P_2- and PtdIns(3,5)P_2-containing vesicles. We then prepared and characterized a triple-site mutant (R1225A/K1229A/K1232A). Interestingly, the mutant exhibited a relatively modest three-fold reduction in affinity for POPC/POPE/PtdIns(3)P (77:20:3) vesicles, indicating that these residues are more likely involved in nonspecific membrane adsorption than specific PI recognition. Indeed, the R1225A/K1229A/K1232A mutant had 10-fold lower affinity than the wild-type KIF16B-PX, for more anionic POPC/POPS/PtdIns(3)P (77:20:3) vesicles (data not shown). Our interpretation of the SPR data is further supported by the monolayer penetration properties of these mutants. As shown in Figure 3B, the R1225A/K1229A/K1232A mutation had a minimal effect on the penetration of KIF16B-PX into the POPC/POPE/PtdIns(3)P (77:20:3) monolayer, whereas both R1220A and R1260A mutations reduced the penetration of KIF16B-PX into the POPC/POPE/PtdIns(3)P (77:20:3) monolayer to the level of its penetration into POPC/POPE (80:20) monolayer.

Mechanism of PI-induced membrane penetration of KIF16B-PX

We have shown for many PI-binding domains that binding of a cognate PI molecule specifically induces the membrane penetration of the protein, by electrostatically neutralizing the excessive positive electrostatic potential of the membrane binding surface and/or inducing local conformational changes near the membrane binding surface (Stahelin *et al*, 2002, 2003a; Cho and Stahelin, 2005). Although KIF16B-PX has high intrinsic membrane penetrating activity, as witnessed by its strong interaction with the POPC/POPE (80:20) monolayer, the activity is significantly enhanced by the presence of 3 mol% PtdIns(3)P in the monolayer, and this increase is abrogated by the mutation of R1220 and R1260 that appear to be involved in PtdIns(3)P ligation. Due to the presence of multiple cationic residues in and around the lipid-binding pocket, the membrane-binding surface of KIF16B has a strong positive electrostatic potential that surrounds the hydrophobic side chains of L1248 and F1249 in the absence of bound PtdIns(3)P (Figure 4A and B). This positive potential, while promoting the initial binding of the protein to the anionic membrane surface, would interfere with the membrane penetration of L1248 and F1249 because the process would involve energetically unfavorable dehydration. As shown in Figure 4C, the binding of PtdIns(3)P to the pocket reduces the positive electrostatic potential near the hydrophobic residues, allowing their side chains to be exposed over the electrostatic potential barrier. This should lead to the enhanced penetration of the hydrophobic side chains into the membrane, as evidenced by our monolayer and SPR data.

Roles of exposed hydrophobic residues in endosomal localization of KIF16B

KIF16B kinesin has been shown to modulate the early endosomal receptor recycling and degradation in a Rab5-dependant manner in HeLa cells (Hoepfner *et al*, 2005). The critical role of the PX domain in endosomal localization and endosomal transport of KIF16B was demonstrated by the loss of cellular activity by the PtdIns(3)P depletion (Hoepfner *et al*, 2005). To determine the physiological significance of our *in vitro* membrane binding data underscoring the importance of hydrophobic residues, L1248 and F1249, we transfected A431 cells with the N-terminal Myc-tagged full-length KIF16B and L1248A/F1249A mutant. Immunoblotting analysis of the same number of cells expressing the wild type

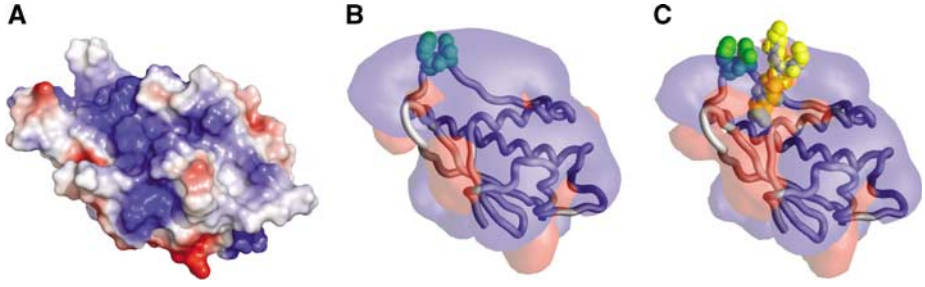

Figure 4 Electrostatic potential calculations of KIF16B-PX. (**A**) The electrostatic potential surface of KIF16B-PX. Red and blue qualitatively indicate negative and positive electrostatic potentials, respectively. (**B**) Worm diagrams of KIF16B-PX backbone are overlayed with a transparent electrostatic potential cloud. L1248 and F1249 (shown in green) are within the positive electrostatic potential cloud, when unligated. (**C**) Bound PtdIns(3)P (shown in yellow) neutralizes some of the positive potential, allowing L1248 and F1249 to rise above.

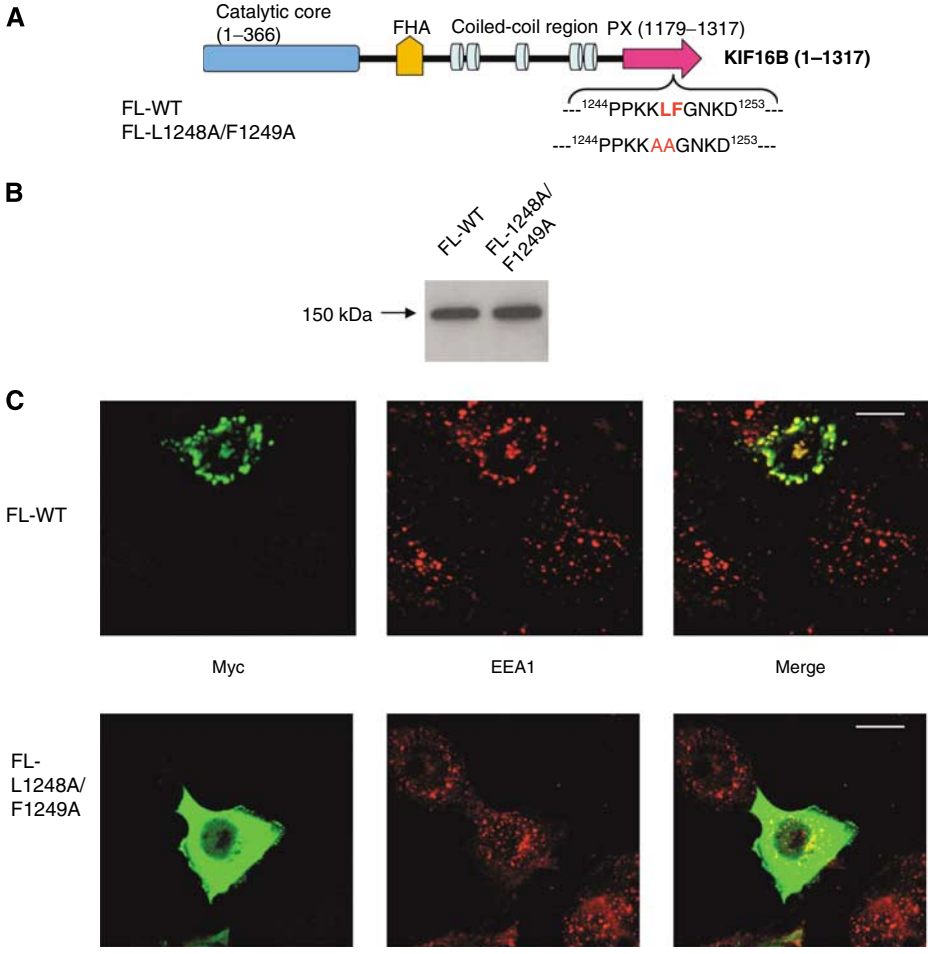

Figure 5 Expression and subcellular localization of the intact KIF16B and the L1248A/F1249A mutant in A431 cells. (**A**) A schematic representation of the full-length (FL) KIF16B structure. (**B**) Constructs for FL-wild type (WT) and the L1248A/F1249A mutant were transfected into A431 cells, and the resulting cell lysates were processed to detect the Myc-tagged proteins by immunoblotting. (**C**) Cells transfected with the constructs for FL-WT and FL-L1248A/F1249A were processed for indirect immunofluorescence microscopy to detect the Myc-tagged proteins as well as endogenous EEA1 (an early endosomal marker). The merged images are also shown. EEA1-positive endosomes were fully (>98%) colocalized with FL-WT, and the expression of FL-WT caused some clustering of endosomes to the cell periphery when compared with non-transfected cells. The L1248A/F1249A mutation disrupted endosomal targeting of KIB16B. In this case, cellular distribution of endosomes was essentially the same in L1248A/F1249A-transfected and non-transfected cells. Images are shown on the same scale. The scale bar indicates 10 μm.

and the mutant showed that the two proteins were expressed at comparable levels (Figure 5B). Immunofluorescence microscopy analysis of >200 fixed A431 cells using an Myc antibody revealed that >98% of full-length KIF16B spots were colocalized with the endogenous EEA1, which is an early endosomal marker, demonstrating the predominant endosomal localization of KIF16B (Figure 5C). Furthermore, expression of the full-length KIF16B caused some degree of clustering of EEA1-positive endosomes to the cell periphery, which is consistent with the physiological role of KIF16B as a kinesin that transports early endosomes to the plus end of microtubules. Most important, the L1248A/F1249A mutation abrogated the endosomal localization of the full-length KIF16B in A431 cells and expression of L1248A/F1249A in A431 cells did not change the cellular distribution of EEA1-positive endosomes. This corroborates the notion that the uniquely exposed hydrophobic residues of KIF16B-PX are a key structural determinant of cellular endosomal anchoring of KIF16B.

To further investigate the specific roles of L1248 and F1249 in endosomal localization of KIF16B, we prepared wild type and mutants of KIF16B-PX containing a C-terminal enhanced green fluorescent protein (EGFP) tag and measured their localization in live HEK293 cells. To establish that KIF16B-PX is also localized at endosomes in HEK293 cells, we first performed dual immunofluorescence staining of expressed KIF16B-PX and endogenous EEA1 using fixed HEK293 cells. In agreement with A431 cell localization, KIF16B-PX was colocalized with endogenous EEA1 (Figure 6A). In live HEK293 cells, KIF16B-PX clearly displayed a punctuate endosomal localization pattern, whereas mutants with greatly reduced affinity for PtdIns(3)P-containing vesicles (i.e., R1220A, R1260A, and L1248A/F1249A; see Table I) were evenly distributed in the cytosol (Figure 6B). Interestingly, three single-site mutants, L1248A, L1248V, and F1249A, which had 7- to 5-fold lower membrane affinity than the wild type, were also found in the cytosol (Figure 6B). This was not due to low expression of these mutants in

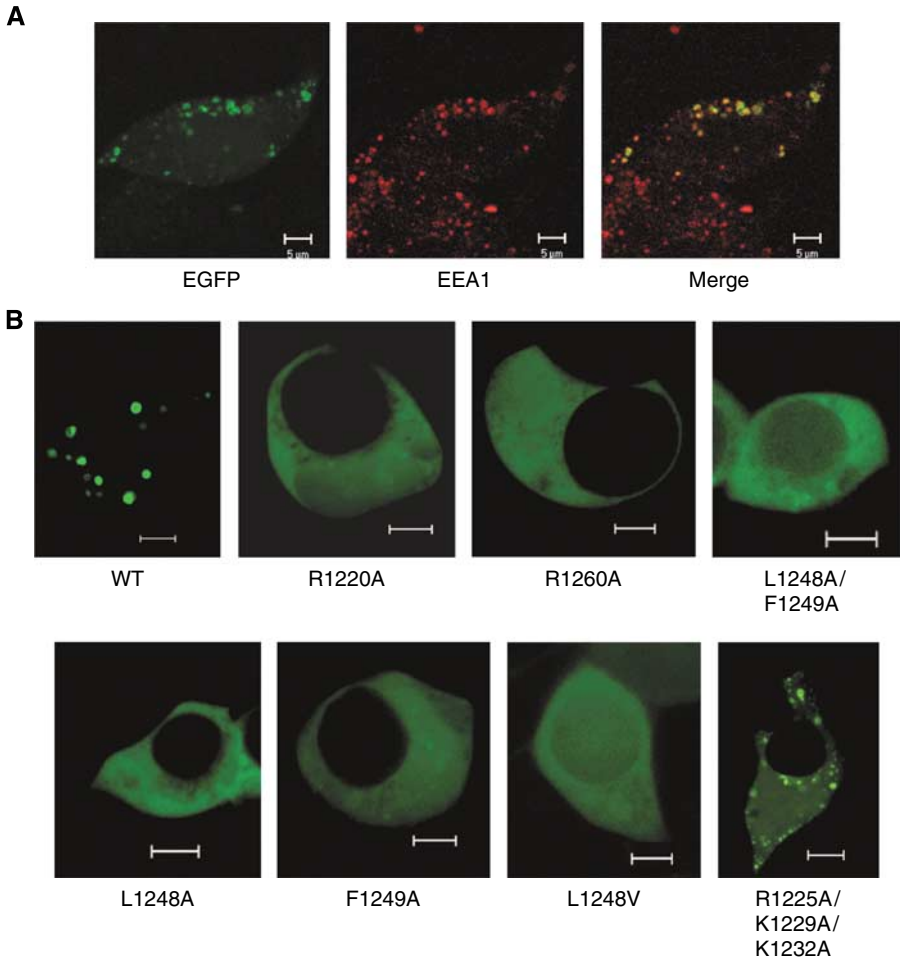

Figure 6 Subcellular localization of KIF16B-PX and its mutants in HEK293 cells. (**A**) Cells transfected with the EFGP-tagged KIF16B-PX construct were processed for immunofluorescence microscopy to detect the endogenous EEA1. (**B**) Imaging of live HEK293 cells transfected with KIF16B-PX and mutants. Each single-cell image shown here represents >70% of cell populations that express similar levels of proteins and display similar subcellular localization patterns. Scale bars indicate 5 μm.

HEK293 cells, because protein expression levels, estimated either by immunoblotting using an EGFP antibody or by the fluorescence correlation spectroscopy analysis (Sanchez and Gratton, 2005) of cell images, were comparable for all PX domain-transfected cells (data not shown). The endosomal localization of another mutant, R1225A/K1229A/K1232A, which has higher membrane affinity than either L1249A or F1249A (Table I) also serves as a positive control establishing that the cytosolic localization of the above PX domain mutants are due specifically to their reduced membrane affinity (Figure 6B). These results thus indicate that the presence of both L1248 and F1249 are crucial for cellular functions of KIF16B and its PX domain.

Discussion

Modulation of endosomal transport by KIF16B is an important process that links PtdIns(3)P, a product of the PI 3-kinase pathway, to intracellular transport, vesicle trafficking, and cell signaling. KIF16B is the only known motor protein that directly interacts with PtdIns(3)P. Strong dependence of KIF16B-mediated endosomal transport on PtdIns(3)P and the lack of other prominent KIF16B–cargo interactions support the notion that PtdIns(3)P–PX interaction is the main driving force for the motor–cargo binding (Hoepfner *et al*, 2005). FYVE and PX domains are two major types of PtdIns(3)P-binding domains and many cellular proteins that interact with PtdIns(3)P-containing early endosomes have one or more of these domains (Birkeland and Stenmark, 2004; Cho and Stahelin, 2005; Seet and Hong, 2006). While FYVE domains specifically bind PtdIns(3)P, PX domains also bind other PIs. This variable specificity is achieved through the structural variation in and near the PI-binding pocket. The KIF16B-PX domain binds all 3-phosphate-containing PIs with relatively high affinity, although it prefers PtdIns(3)P to other 3-PIs by >10-fold. This is unusual even for PX domains because PX domains in general have high affinity for one, or at most two, PIs (Seet and Hong, 2006). Our crystal structure shows that this broad PI selectivity of KIF16B-PX is ascribed to its PI-binding pocket that is more open than those of other PtdIns(3)P-specific PX domains such as $p40^{phox}$-PX. Although we could not pinpoint the residues involved in stereospecific recognition of the PI headgroup, due to difficulties encountered in obtaining KIF16B-PX–PI complexes, structural comparison with $p40^{phox}$-PX as well as our mutational analysis suggest that R1220 is a key ligand for the 3-phosphate, whereas R1260 is involved in interaction with the 4- and 5-phosphate. The physiological significance of broad 3-PI

specificity of KIF16B-PX is not known at present. Taking into account the low cellular abundance of PtdIns(3,4)P_2, PtdIns(3,5)P_2, and PtdIns(3,4,5)P_3, and the presence of other lipid-binding domains that specifically bind each of these 3-PIs with higher affinity, direct binding of KIF16B-PX to 3-PIs other than PtdIns(3)P may not be physiologically significant. It is possible, however, that affinity for these 3-PIs may contribute to the membrane interaction of KIF16B-PX in response to a surge in local concentration of 3-PIs under certain conditions.

A large number of PtdIns(3)P-specific FYVE and PX domains do not have affinity high enough for PtdIns(3)P-containing vesicles to achieve autonomous localization at early endosomes, when expressed as isolated domains in mammalian cells (Birkeland and Stenmark, 2004; Blatner *et al*, 2004; Cho and Stahelin, 2005; Kutateladze, 2006). Thus, the endosomal localization of the proteins harboring low-affinity FYVE and PX domains (e.g., EEA1) requires protein dimerization and/or interactions with endosomal proteins (Birkeland and Stenmark, 2004). A systematic comparison of the affinity of a large number of FYVE domain constructs for PtdIns(3)P-containing vesicles and their subcellular localization revealed that the K_d for PtdIns(3)P-containing vesicles must be higher than a threshold value for a domain to be localized at early endosomes in HEK293 cells (Blatner *et al*, 2004). The K_d of KIF16B-PX for POPC/POPE/PtdIns(3)P (77:20:3) is comparable to those of the FYVE domains of FENS-1 and endofin, which tightly bind as monomers to vesicles and are localized at early endosomes in HEK293 cells (Blatner *et al*, 2004). The K_d value is also comparable to that of p40^{phox}-PX, which is also endosomally localized in HEK293 cells (Stahelin *et al*, 2003a). Therefore, KIF16B-PX has high affinity for PtdIns(3)P-containing vesicles that would allow its tight interactions with early endosomes. It has been suggested that KIF16B may form a dimer because of the presence of putative coiled coil motifs. Our fluorescence correlation spectroscopy measurement of the EGFP-tagged KIF16B-PX indicates that it does not form a dimer either in solution or on the membrane (NR Blatner and W Cho, unpublished observation). Whether full-length KIF16B forms a dimer or not, an individual PX domain of KIF16B should provide membrane binding strong enough to tether KIF16B to early endosomes.

Although high-affinity binding to PtdIns(3)P-containing vesicles has been seen with other FYVE and PX domains, extremely slow membrane dissociation kinetics of KIF16B-PX is unique among these domains. In addition to the specific PI binding, PI-binding domains can achieve high affinity through nonspecific electrostatic interactions and hydrophobic interactions that generally involve the membrane penetration of hydrophobic residues. The former generally accelerates the membrane association, whereas the latter slows the membrane dissociation (Cho and Stahelin, 2005). Our structural and mutational studies suggest that sustained membrane residence of KIF16B-PX is attributed to L1248 and F1249 that are uniquely positioned on the membrane-binding surface of KIF16B-PX and penetrate into the hydrocarbon region of the membrane. The presence of multiple hydrophobic residues on the membrane-binding surface is common among lipid-binding domains, and many of these residues are situated next to each other in PX domains and contribute to membrane binding (Cheever *et al*, 2001; Stahelin *et al*, 2003a; Lee *et al*, 2006). To date, however, no lipid-binding domain has been reported to have two hydrophobic side chains forming such a conspicuously protruding hydrophobic stalk with a large solvent accessible surface area. This unique structure arises from the local conformation surrounding L1248 and F1249, and the complementary stacking of the two side chains. Complete burial of the exposed hydrophobic surface of these residues in the membrane could contribute up to 3.5 kcal/mol of stabilization energy, which would greatly enhance the membrane affinity of the PX domain and slow membrane dissociation. Although we have not determined the depth of membrane penetration by KIF16B-PX, large negative effects of single and double-site mutations of L1248 and F1249 on membrane binding suggest that these residues fully penetrate into the hydrocarbon region of the lipid bilayer.

The membrane affinity of the L1248F/F1249L mutant (Table I), which is similar to the wild type, indicates that it is the total surface area of the two complementary hydrophobic side chains at these positions, rather than the particular residues present, that determines the membrane binding activity of the KIF16B-PX domain. Although the importance of hydrophobic residues in membrane binding of proteins has been well documented (White and Wimley, 1998; Cho and Stahelin, 2005), mutation of a single hydrophobic residue rarely has a dramatic effect on either *in vitro* membrane affinity or subcellular translocation, as is the case for L1248A, L1248V, or F1249A. This suggests that the total surface area (270 Å^2) of the hydrophobic side chains at these positions should only be slightly above a threshold value for the KIF16B-PX domain, to ensure optimal association with early endosomes.

In summary, the present study elucidates the structural basis of the endosomal anchoring of a recently identified kinesin, KIF16B. This is a unique KIF in that its cargo interaction is primarily driven by membrane–protein interactions. The unique membrane binding mechanism of this PX domain, which depends largely on hydrophobic interactions, fits well the physiological function of KIF16B that not only binds early endosomes but also transports them along microtubules. There are many structurally uncharacterized lipid-binding domains that have proximal hydrophobic pairs on their putative membrane binding surfaces. For instance, an Φ-Φ-G motif (Φ = hydrophobic residue) has been found on the PP_{II}–α2 loop of 12 out of 47 known mammalian PX domains, including PX domains of p40^{phox}, PI3K-C2α, CISK, sorting nexins 1, 2 8, 9, 11, 14, 15, and 29 (Supplementary Figure 2). Thus, the unique local structure of KIF16B-PX may represent a general structural strategy used by the proteins whose function in membrane trafficking depends on strong hydrophobic interactions.

Materials and methods

cDNA cloning and mutagenesis

The coding region of human KIF16B was retrieved by PCR from human EST clone (GenBank accession number BX647572, clone ID DKFZp313B0719; Invitrogen). The PCR products were digested with enzymes *Xho*I and *Not*I, and resolved by agarose gel electrophoresis. The desired DNA fragment was subcloned into pDMyc-neo vector, which is a modified version of the pCI-neo vector (Stratagene) with two Myc epitope sequences inserted 5′ to the multiple cloning site (Seet and Hong, 2001). An Myc-tagged point

mutant (L1248A/F1249A) of the full-length KIF16B was generated by PCR. The PX domain and mutants without the Myc tag were also subcloned into a modified pIND vector to prepare the constructs with the C-terminal EGFP, as described previously (Stahelin *et al*, 2003b).

Protein expression

The PX domains containing a C-terminal His_6 tag were expressed and purified as described previously (Stahelin *et al*, 2003a), with a minor variation: that is, the domains purified by Ni^{2+}-affinity chromatography were further purified by ion-exchange chromatography using a S-Sepharose column. The purified protein was concentrated in 20 mM Tris–HCl, pH 7.4, containing 0.16 M KCl. Protein concentration was then determined by the bicinchoninic acid method (Pierce). For crystallization, the His_6-tagged KIF16B-PX domain was overexpressed in an *Escherichia coli* methionine auxotrophic strain, B834(DE3)pLysS (Novagen). Cultures were grown at 18°C overnight in complete M9 minimal growth media supplemented with 40 μg/l seleno-L-Met and induced by 0.3 mM isopropyl β-D-1-thiogalactopyranoside when the optical density (600 nm) of the culture reached the value of 1. The protein was purified as described in the Supplementary data. The protein was then concentrated in 20 mM Tris pH 8.0 with 100 mM NaCl and 2 mM DTT to 7.4 mg/ml and flash frozen in liquid N_2 and stored at −80°C. The protein was thawed on ice for 1 h immediately before use in crystallization trials.

Crystallization

Crystals of KIF16B-PX domain, substituted with seleno-L-Met, were initially obtained from screening 1440 crystallization solutions dispensed robotically (Innovadyne) as sitting drops into 96-well plates (MRC), and incubated at 17°C. After optimization, crystals of KIF16B-PX were grown by hair-seeding sitting drops containing 2 μl of protein, 500 μM di-C_4 PtdIns(3,4,5)P_3 (Echelon), and 1 μl of reservoir solution (25% PEG 3350, 0.1 M Tris pH 8.8, 0.2 M NH_4OAc). The drops were then incubated at 17°C over a reservoir solution for 4 days. Before collecting X-ray diffraction data, crystals were soaked in cryoprotectant (25% PEG 3350, 0.1 M Tris pH 8.8, 0.2 M NH_4OAc, 20% glycerol) for 1 min and frozen in nitrogen gas at 100 K.

Structure determination and refinement

Two X-ray diffraction data sets for phasing using multi-wavelength anomalous dispersion, one at 0.979 Å (peak) and another at 0.939 Å (remote), were collected at 100 K on beamline ID14-4 at the European Synchrotron Radiation Facility, using an ADSC CCD detector. The data were integrated and scaled to 2.2 Å using MOSFLM and SCALA programs. The crystals belonged to space group I23 with unit-cell dimensions of $a = 100.9$ Å and contain one molecule in the asymmetric unit. The positions for two of three selenium atoms per molecule were determined using the HySS (hybrid sub-structure search) module of PHENIX and refined using autoSHARP, with no additional sites being found. The FOM was 0.30, with an overall phasing power for isomorphous differences of 1.06, and for anomalous differences it was 0.904. After solvent flattening was carried out by SOLOMON, using a solvent content optimized by SHARP, the FOM was 0.89, and after DM it was 0.91. An initial model was built by Arp/WARP, and refined by REFMAC5, with alternating rounds of manual rebuilding using the program COOT. Final statistics for the 2.2 Å model, encompassing residues 1179–1317 of KIF16B, are provided in Table II. Electron density is poor for residues 1196–1199 on the β1–β2 loop that faces the solvent in the crystal. With the exception of L1211, which is located on a very tight turn, for which there is excellent electron density, all other residues are within allowed regions of the Ramachandran plot generated by PROCHECK (95.9% most favored, 3.3% additionally allowed, 0% generously allowed, and 0.8% disallowed). Solvent accessible surface area of L1248 and F1249 side chains were calculated with AREAIMOL using an atomic radius for C of 1.87 Å and a probe size for water of 1.4 Å.

Monolayer measurements

Surface pressure (π) was measured using a Wilhelmy plate as described in the Supplementary data. Briefly, the equilibrium change in surface pressure (Δπ) of a phospholipid monolayer with a given initial pressure (π_0) was measured following injection of protein into the subphase (20 mM Tris–HCl, pH 7.4, 0.16 M KCl). The π_c was determined by extrapolating the Δπ versus π_0 plot to the *x*-axis.

SPR measurements

All SPR measurements were performed at 23°C and in 20 mM Tris–HCl, pH 7.4, containing 0.16 M KCl using a lipid-coated L1 chip in the BIACORE X system, as described in the Supplementary data.

Electrostatic potential calculations

The electrostatic properties of the KIF16B-PX domain with and without bound lipid were calculated with a modified version of the program Delphi and visualized in the program GRASP (Nicholls *et al*, 1991). The electrostatic potential calculations performed used partial charges taken from the CHARMM27 force field (Brooks *et al*, 1983) and spatial coordinates from the structure of KIF16B-PX. Inositol-1,3-bisphosphate was docked to KIF16B-PX using superposition of $p40^{phox}$-PX (PDB id: 1H6H; Bravo *et al*, 2001) with KIF16B-PX and copying the coordinates of KIF16B-PX from the superposition and those of the ligand from 1H6H. Steric clashes were fixed manually.

Immunofluorescence confocal microscopy in HeLa cells

A431 cells were grown in DMEM supplemented with 10% fetal bovine serum (Gibco) in a 5% CO_2 incubator at 37°C. Transfection was performed using Lipofectamine™ 2000 (Invitrogen). Cells were processed for immunofluorescence, or Western blot, 24 h after transfection. A431 cells, grown on coverslips, were fixed with paraformaldehyde (3% in PBS) for 20 min at room temperature, and then permeabilized with 0.1% (w/v) saponin in PBSCM (PBS containing 1 mM $CaCl_2$ and 1 mM $MgCl_2$) for 30 min at room temperature, before incubation with the indicated primary antibodies. All primary and secondary antibody incubations were performed in fluorescence dilution buffer (FDB: 5% fetal calf serum, 5% goat serum, and 2% BSA in PBSCM). After mounting, the cells were viewed by using a Zeiss LSM 510 laser scanning confocal microscope (Zeiss).

Live cell imaging in HEK293 cells

A stable HEK293 cell line expressing the ecdysone receptor (Invitrogen) was used for live cell imaging, as described previously (Stahelin *et al*, 2003b). Imaging was performed with a Zeiss LSM510 microscope with the laser intensity, the pinhole size, and the detector gain kept at the same setting. A linepass 505-nm filter and a 63×1.2 numerical aperture water-immersion objective were used for all experiments. EGFP was excited using the 488 line of an Argon/Krypton laser. Transfected cells were washed twice with 1 mM HEPES, buffer pH 7.4, containing 2.5 mM $MgCl_2$, 140 mM NaCl, 5 mM KCl, and 6 mM sucrose. After washing, cells were overlaid with 150 μl of the same buffer. Representative cells were selected and a single image was taken for each cell.

Immunoblotting

Proteins separated by SDS–polyacrylamide electrophoresis were transferred onto nitrocellulose membranes (Hybond-C; Amersham Biosciences). Membranes were incubated 1 h at room temperature with the primary antibody. Membranes were washed three times for 10 min each in PBST (PBS containing 0.05% Tween 20) and exposed for 1 h at room temperature with secondary antibodies. Proteins were detected using the SuperSignal West Pico Chemiluminescence Substrate.

Accession codes

Protein Data Bank: coordinates and structure factors will be deposited with PDB.

Supplementary data

Supplementary data are available at *The EMBO Journal* Online (http://www.embojournal.org).

Acknowledgements

MIW and RLW are grateful to David Gill, Elsbeth Gordon, and Andrew McCarthy for help with data collection at ESRF Beamline ID14-4. This study was supported by grants from National Institutes of Health (GM68849 for WC and GM66147 for DM). MIW is supported by a Fellowship from the British Heart Foundation.

References

Birkeland HC, Stenmark H (2004) Protein targeting to endosomes and phagosomes via FYVE and PX domains. *Curr Top Microbiol Immunol* **282:** 89–115

Blatner NR, Stahelin RV, Diraviyam K, Hawkins PT, Hong W, Murray D, Cho W (2004) The molecular basis of the differential subcellular localization of FYVE domains. *J Biol Chem* **279:** 53818–53827

Bravo J, Karathanassis D, Pacold CM, Pacold ME, Ellson CD, Anderson KE, Butler PJ, Lavenir I, Perisic O, Hawkins PT, Stephens L, Williams RL (2001) The crystal structure of the PX domain from p40(phox) bound to phosphatidylinositol 3-phosphate. *Mol Cell* **8:** 829–839

Brooks B, Bruccoleri R, Olafson B, States D, Swaminathan S, Karplus M (1983) CHARMM: a program for macromolecular energy, minimization, and dynamics calculations. *J Comp Chem* **4:** 187–217

Caviston JP, Holzbaur EL (2006) Microtubule motors at the intersection of trafficking and transport. *Trends Cell Biol* **16:** 530–537

Cheever ML, Sato TK, de Beer T, Kutateladze TG, Emr SD, Overduin M (2001) Phox domain interaction with PtdIns(3)P targets the Vam7 t-SNARE to vacuole membranes. *Nat Cell Biol* **3:** 613–618

Cho W, Stahelin RV (2005) Membrane-protein interactions in cell signaling and membrane trafficking. *Annu Rev Biophys Biomol Struct* **34:** 119–151

Chothia C (1974) Hydrophobic bonding and accessible surface area in proteins. *Nature* **248:** 338–339

Demel RA, Geurts van Kessel WS, Zwaal RF, Roelofsen B, van Deenen LL (1975) Relation between various phospholipase actions on human red cell membranes and the interfacial phospholipid pressure in monolayers. *Biochim Biophys Acta* **406:** 97–107

Gillooly DJ, Morrow IC, Lindsay M, Gould R, Bryant NJ, Gaullier JM, Parton RG, Stenmark H (2000) Localization of phosphatidylinositol 3-phosphate in yeast and mammalian cells. *EMBO J* **19:** 4577–4588

Hoepfner S, Severin F, Cabezas A, Habermann B, Runge A, Gillooly D, Stenmark H, Zerial M (2005) Modulation of receptor recycling and degradation by the endosomal kinesin KIF16B. *Cell* **121:** 437–450

Horiguchi K, Hanada T, Fukui Y, Chishti AH (2006) Transport of PIP3 by GAKIN, a kinesin-3 family protein, regulates neuronal cell polarity. *J Cell Biol* **174:** 425–436

Karathanassis D, Stahelin RV, Bravo J, Perisic O, Pacold CM, Cho W, Williams RL (2002) Binding of the PX domain of p47(phox) to phosphatidylinositol 3,4-bisphosphate and phosphatidic acid is masked by an intramolecular interaction. *EMBO J* **21:** 5057–5068

Klopfenstein DR, Tomishige M, Stuurman N, Vale RD (2002) Role of phosphatidylinositol(4,5)bisphosphate organization in membrane transport by the Unc104 kinesin motor. *Cell* **109:** 347–358

Kutateladze TG (2006) Phosphatidylinositol 3-phosphate recognition and membrane docking by the FYVE domain. *Biochim Biophys Acta* **1761:** 868–877

Lee JR, Shin H, Choi J, Ko J, Kim S, Lee HW, Kim K, Rho SH, Lee JH, Song HE, Eom SH, Kim E (2004) An intramolecular interaction between the FHA domain and a coiled coil negatively regulates the kinesin motor KIF1A. *EMBO J* **23:** 1506–1515

Lee SA, Kovacs J, Stahelin RV, Cheever ML, Overduin M, Setty TG, Burd CG, Cho W, Kutateladze TG (2006) Molecular mechanism of membrane docking by the Vam7p PX domain. *J Biol Chem* **281:** 37091–37101

Lu J, Garcia J, Dulubova I, Sudhof TC, Rizo J (2002) Solution Structure of the Vam7p PX Domain. *Biochemistry* **41:** 5956–5962

Marsh D (1996) Lateral pressure in membranes. *Biochim Biophys Acta* **1286:** 183–223

Miki H, Okada Y, Hirokawa N (2005) Analysis of the kinesin superfamily: insights into structure and function. *Trends Cell Biol* **15:** 467–476

Nicholls A, Sharp KA, Honig B (1991) Protein folding and association: insights from the interfacial and thermodynamic properties of hydrocarbons. *Proteins* **11:** 281–296

Sanchez SA, Gratton E (2005) Lipid–protein interactions revealed by two-photon microscopy and fluorescence correlation spectroscopy. *Acc Chem Res* **38:** 469–477

Seet LF, Hong W (2001) Endofin, an endosomal FYVE domain protein. *J Biol Chem* **276:** 42445–42454

Seet LF, Hong W (2006) The Phox (PX) domain proteins and membrane traffic. *Biochim Biophys Acta* **1761:** 878–896

Stahelin RV, Burian A, Bruzik KS, Murray D, Cho W (2003a) Membrane binding mechanisms of the PX domains of NADPH oxidase p40phox and p47phox. *J Biol Chem* **278:** 14469–14479

Stahelin RV, Karathanassis D, Bruzik KS, Waterfield MD, Bravo J, Williams RL, Cho W (2006) Structural and membrane binding analysis of the Phox homology domain of phosphoinositide 3-kinase-C2alpha. *J Biol Chem* **281:** 39396–39406

Stahelin RV, Long F, Diraviyam K, Bruzik KS, Murray D, Cho W (2002) Phosphatidylinositol 3-phosphate induces the membrane penetration of the FYVE domains of Vps27p and Hrs. *J Biol Chem* **277:** 26379–26388

Stahelin RV, Rafter JD, Das S, Cho W (2003b) The molecular basis of differential subcellular localization of C2 domains of protein kinase C-alpha and group IVa cytosolic phospholipase A2. *J Biol Chem* **278:** 12452–12460

Westerholm-Parvinen A, Vernos I, Serrano L (2000) Kinesin subfamily UNC104 contains a FHA domain: boundaries and physicochemical characterization. *FEBS Lett* **486:** 285–290

White SH, Wimley WC (1998) Hydrophobic interactions of peptides with membrane interfaces. *Biochim Biophys Acta* **1376:** 339–352

Wimley WC, White SH (1996) Experimentally determined hydrophobicity scale for proteins at membrane interfaces. *Nat Struct Biol* **3:** 842–848

Wishart MJ, Taylor GS, Dixon JE (2001) Phoxy lipids: revealing PX domains as phosphoinositide binding modules. *Cell* **105:** 817–820

Xing Y, Liu D, Zhang R, Joachimiak A, Songyang Z, Xu W (2004) Structural basis of membrane targeting by the Phox homology domain of cytokine-independent survival kinase (CISK-PX). *J Biol Chem* **279:** 30662–30669

Zhou CZ, de La Sierra-Gallay IL, Quevillon-Cheruel S, Collinet B, Minard P, Blondeau K, Henckes G, Aufrere R, Leulliot N, Graille M, Sorel I, Savarin P, de la Torre F, Poupon A, Janin J, van Tilbeurgh H (2003) Crystal structure of the yeast Phox homology (PX) domain protein Grd19p complexed to phosphatidylinositol-3-phosphate. *J Biol Chem* **278:** 50371–50376